Louisiana State University
LSU Digital Commons

2015

Near Total Resonant Light Absorption in a Graphene Monolayer at Multiple Tunable Wavelengths with Multilayer Structures

Iman Zand

Louisiana State University and Agricultural and Mechanical College, izand1@lsu.edu

NEAR TOTAL RESONANT LIGHT ABSORPTION IN A GRAPHENE
MONOLAYER AT MULTIPLE TUNABLE WAVELENGTHS WITH
MUTILAYER STRUCTURES

A Thesis

Submitted to the Graduate Faculty of the
Louisiana State University and
Agricultural and Mechanical College
in partial fulfillment of the
requirements for the degree of
Master of Science

in

The Department of Electrical and Computer Engineering

by
Iman Zand
B.Sc., K. N. Toosi University, 2011
December 2015

Dedicated to

Dr. Georgios Veronis

ACKNOWLEDGEMENTS

TABLE OF CONTENTS

ABSTRACT

Graphene could be potentially important for a broad range of photonic and optoelectronic applications. For such graphene-based applications it is critical to enhance the absorption of light in graphene monolayers in order to achieve near total absorption. Several structures have been proposed to enhance light absorption in graphene at visible and infrared wavelengths such as one-dimensional Fabry-Perot cavity structures, and photonic crystal slabs. Fabry-Perot cavity structures, which employ periodic Bragg mirrors, can lead to near total light absorption on resonance. However, such structures cannot achieve near complete absorption in graphene at multiple closely-spaced tunable wavelengths, which is potentially important for applications requiring multispectral light detection.

In this thesis, we consider a one-dimensional system for enhancing the absorption in a graphene monolayer at multiple tunable wavelengths. The graphene monolayer is sandwiched between two aperiodic multilayer structures composed of alternating layers of silicon and silica. The structure is deposited on a silica substrate. We show that such a system can achieve near total resonant light absorption in graphene at multiple tunable wavelengths.

1.1 Properties of Graphene

Graphene is a single atomic layer of graphite; an abundant mineral which is an allotrope of carbon that is made up of very tightly bonded carbon atoms organized into a hexagonal lattice. What makes graphene so special is its sp^2 hybridization (Figure 1.1) and very thin atomic thickness (~0.345 nm). These properties enable graphene to demonstrate extreme properties in terms of strength, electricity and heat conduction (as well as many others) [1,2].

(a)   (b)
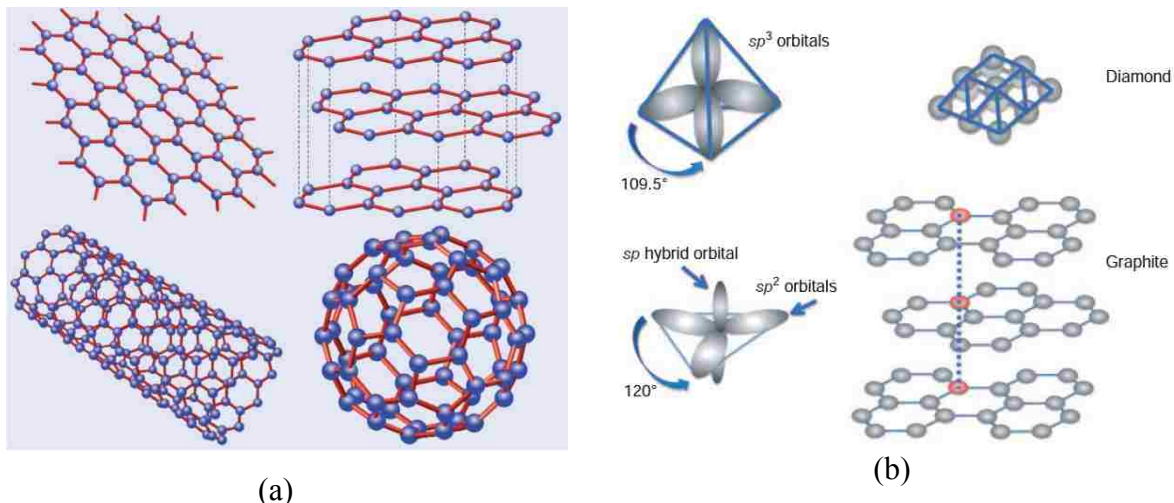
Figure 1.1 (a) Graphene and its descendants: top right: graphene; top left: graphite = stacked graphene; bottom right: nanotube=rolled graphene; bottom left: fullerene=wrapped graphene. (b) Illustration of bonding of carbon in diamond and graphite crystal structures. There are four electrons in each carbon atom that produce bonding with nearest neighbors. In diamond (top) the charge distribution associated with these electrons forms a tetrahedral structure (sp^3 orbitals) around each atom. The atoms thus come together in a tetrahedral arrangement. In graphite (bottom) the bonding electrons form a charge distribution of three equally spaced lobes in a plane (sp^3 orbitals) with the charge distribution of the fourth being out of the plane (sp hybrid orbital) [1].

Before monolayer graphene was isolated in 2004, it was believed that two-dimensional (2-D) compounds could not exist due to thermal instability when separated. However, once graphene was isolated, it became clear that it was actually possible for such compounds to exist. It took scientists some time to identify the mechanisms which enable

these compounds. After suspended graphene sheets were studied by transmission electron microscopy, scientists believed that they identified a mechanism associated with slight rippling in the graphene, which modifies the structure of the material. However, later research suggested that the fact that the carbon to carbon bonds in graphene are so small and strong prevents thermal fluctuations from destabilizing graphene.

Another stand-out property of graphene is its inherent strength. Due to the strength of its 0.142 nm-long carbon bonds, graphene is the strongest material ever discovered, with an ultimate tensile strength of 1.3e11 pascals, compared to 4e8 for A36 structural steel, and 375,700,000 for aramid (Kevlar). Not only is graphene extraordinarily strong, it is also very light with a weight of 0.77 milligrams per square meter. For comparison purposes, one square meter of paper is roughly 1000 times heavier. Thus, a single sheet of graphene (being only 1 atom thick), sufficient enough in size to cover a whole football field, would weigh less than one gram [1,2].

What makes graphene particularly special is that it also exhibits elastic properties, and is able to retain its initial size after strain. In 2007, atomic force microscopy (AFM) tests were carried out on graphene sheets which were suspended over silicon dioxide cavities. These tests showed that graphene sheets (with thicknesses of between 2 and 8 nm) had spring constants in the region of 1-5 N/m and a Young's modulus (different to that of three-dimensional graphite) of 0.5 TPa [2]. It should be noted that these extraordinary properties were obtained for graphene sheets that were unflawed and contained no imperfections. Such structures are currently very expensive and difficult to fabricate. However, fabrication techniques are steadily improving, ultimately reducing costs and complexity.

Graphene's ability to absorb a rather large portion (~2.3%) of incident white light is also a unique and interesting property, especially considering that it is only one atom thick. This is due to its aforementioned electronic properties; the electrons act as massless charge

carriers with very high mobility. A few years ago, it was shown that the amount of white light absorbed by graphene is based on the Fine Structure Constant, rather than being dictated by material specifics [2]. Adding another layer of graphene increases the amount of white light absorbed by approximately the same amount (~2.3%). Graphene's opacity of $\pi\alpha \approx 2.3\%$ is equal to the universal dynamic conductivity value of G = $e^2/4h$ ($\pm$2-3%) over the visible frequency range [3-7]. Here e is the electron charge and h is Planck's constant.

Due to these impressive characteristics, it has been observed that, once optical intensity reaches a certain threshold (known as the saturation fluence), saturable absorption takes place. In other words, light of very high intensity causes a reduction in absorption. This is an important characteristic for applications related to mode-locking of fiber lasers. Due to graphene's properties of wavelength-insensitive ultrafast saturable absorption, full-band mode locking has been achieved using an erbium-doped dissipative soliton fiber laser capable of obtaining wavelength tuning as large as 30 nm [8].

1.2. Applications of Graphene

1.2.1 Energy

Graphene-based nanomaterials have many promising applications in energy-related areas. Here are a few recent examples: Graphene improves both the energy capacity and the charge rate in rechargeable batteries; activated graphene leads to superior supercapacitors for energy storage; graphene electrodes may lead to a promising approach for making solar cells that are inexpensive, lightweight and flexible; and multifunctional graphene mats are promising substrates for catalytic systems [2,3].

1.2.2 Sensing

Functionalized graphene holds exceptional promise for biological and chemical sensors. Researchers have already shown that the distinctive 2-D structure of graphene oxide (GO), combined with its superpermeability to water molecules, leads to sensing devices (Figure 1.2) with an unprecedented speed. Scientists have now found that chemical vapors change the noise spectra of graphene transistors, allowing them to perform selective gas sensing for many vapors with a single device made of pristine graphene. No functionalization of the graphene surface is required for these applications [4].
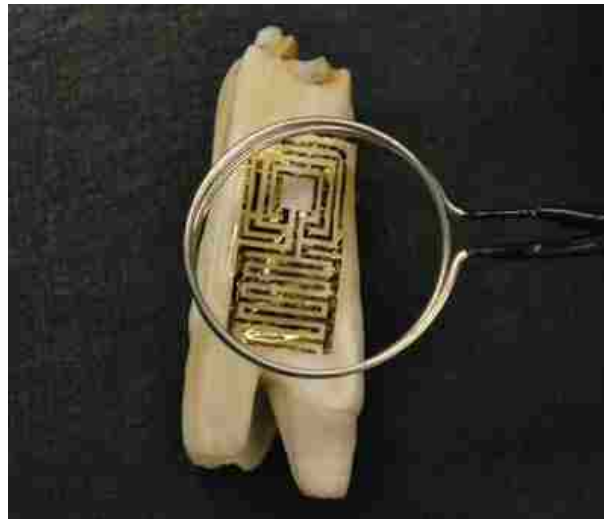
Figure 1.2 Optical image of the graphene wireless sensor biotransferred onto the surface of a tooth (image: McAlpine Group, Princeton University).

1.2.3. Nanoelectronics

Some of the most promising applications of graphene are in electronics (as transistors and interconnects), detectors (as sensor elements), and thermal management (as lateral heat spreaders). The first graphene field-effect transistors (FETs) – with both bottom and top gates – have already been demonstrated. At the same time, for any transistor to be useful for analog communication or digital applications, the level of the electronic low-frequency noise has to be decreased to an acceptable level [5].

Transistors on the basis of graphene are considered to be potential successors for some silicon components currently in use. Due to the fact that an electron can move faster through graphene than through silicon, graphene shows potential to enable terahertz computing. In the ultimate nanoscale transistor, which would be a ballistic transistor, the electrons would avoid collisions, i.e. there would be a virtually unimpeded flow of current. Ballistic conduction would enable incredibly fast switching devices. Graphene has the potential to enable ballistic transistors at room temperature [5,6].

Graphene has the potential to revolutionize electronics and replace the currently used silicon materials. It could lead to high-performance transistors with high mobility at room temperature [5]. However, it does have an Achilles heel: pristine graphene is semi-metallic and lacks the necessary band gap to serve as a transistor. Therefore, it is necessary to engineer band gaps in graphene [5,6].

1.2.4. Photodetectors

Researchers have demonstrated that graphene can be used for telecommunications applications and that its weak and universal optical response might be advantageous for ultrafast photonics applications. They also found that graphene could be potentially exploited as a saturable absorber with wide optical response ranging from ultra-violet, visible, infrared to terahertz [9-13]. There is a very strong research interest in using graphene for applications in optoelectronics. Graphene-based photodetectors have been realized before and graphene's suitability for high bandwidth photodetection has been demonstrated in a 10 GBit/s optical data link [9].

One novel approach is based on the integration of graphene into an optical micro-cavity. The increased electric field amplitude inside the cavity causes more energy to be

absorbed, leading to a significant increase of the photoresponse, as discussed in the next section.

1.3. Enhancing Absorption of Light by Graphene

One of the critical issues in graphene-based applications, especially for light detection, is enhancing the absorption of light in graphene monolayer in order to achieve near total absorption. In the visible and near-infrared range, combining graphene with plasmonic nanostructures (Figure. 1.3) [10] or nanoparticles (Figure. 1.4) [11] can help to increase the absorption of light.
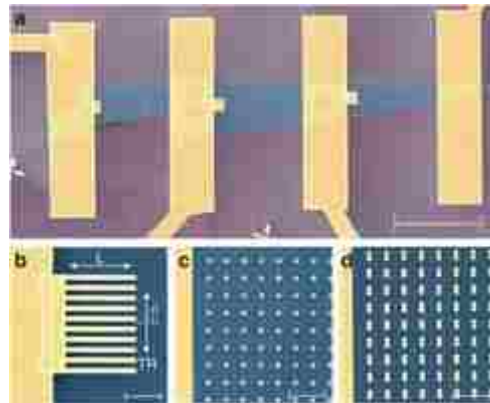
Figure 1.3 Scanning electron microscopy micrographs of the graphene devices with plasmonic nanostructures [10].

(a)   (b)
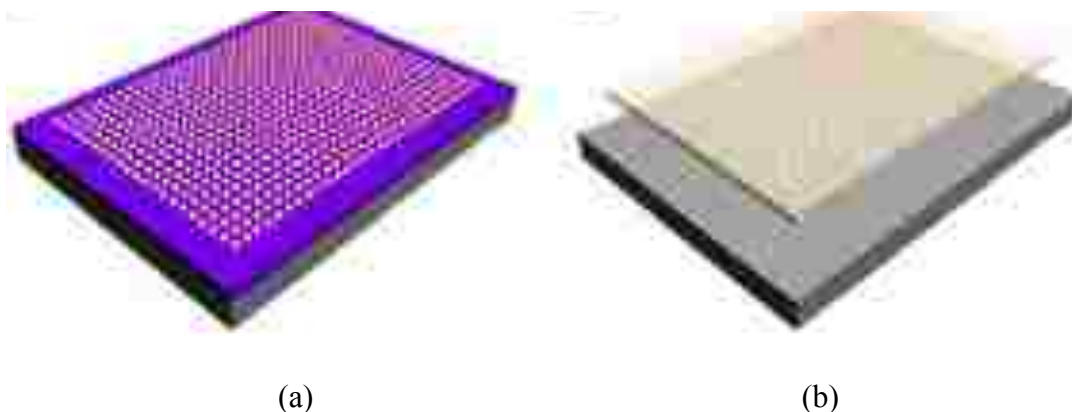
Figure 1.4 Schematic illustration of the fabrication process to integrate plasmonic nanoparticles with graphene. (**a**) Gold nanoparticles are obtained by thermally annealing 4 nm thick gold film on the SiO_2 substrate. (**b**) PMMA is spin coated on the substrate, followed by a lifting-off process using buffered oxide etch to obtain free-standing PMMA/Au [11].

Other approaches to increase absorption of light by graphene monolayer are using one-dimensional (1-D) Fabry-Perot cavity structures [14-21]. In these designs, periodic multilayer structures have been used as optical mirrors. By placing graphene layer inside the cavity or on top or below the cavity nearly 100% percent of light absorption can be achieved. Figure 1.5 shows the general schematic of these structures and also the electric field distribution inside the structure at the wavelength at which absorption is maximized. As seen, the electric field is greatly enhanced near the graphene layer.
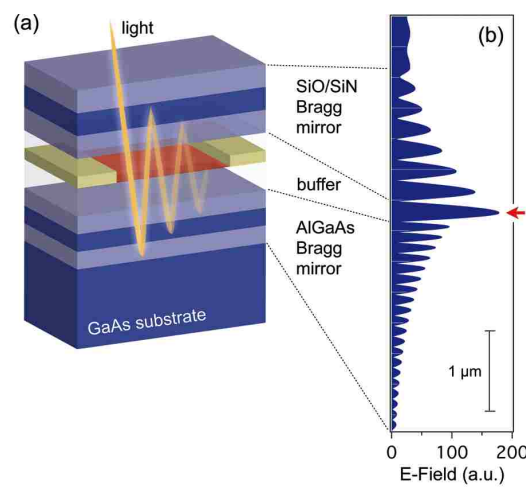
Figure 1.5 (a) Schematic drawing of a graphene microcavity photodetector. Distributed Bragg mirrors form a high-finesse optical cavity. The incident light is trapped in the cavity and passes multiple times through the graphene. The graphene sheet is shown in red, and the metal contacts are in yellow. (b) Electric field amplitude inside the cavity [14].

Recently, photonic crystal slabs in combination with multilayer structures have been used to get near perfect absorption of light (Figure 1.6) [15]. In this design, graphene is placed on the top of the structure which makes the fabrication process easier.

7

Figure 1.6 Schematic of an absorption enhancement system for graphene, using either (a) a lossless metallic mirror or (b) a multilayer dielectric Bragg mirror (1.5 pairs are shown). The high-index dielectric is blue, yellow represents the lossless metal, and green represents a low-index dielectric. In both cases, light is incident normally from above [15].

CHAPTER 2
SIMULATION METHOD

2.1 Introduction

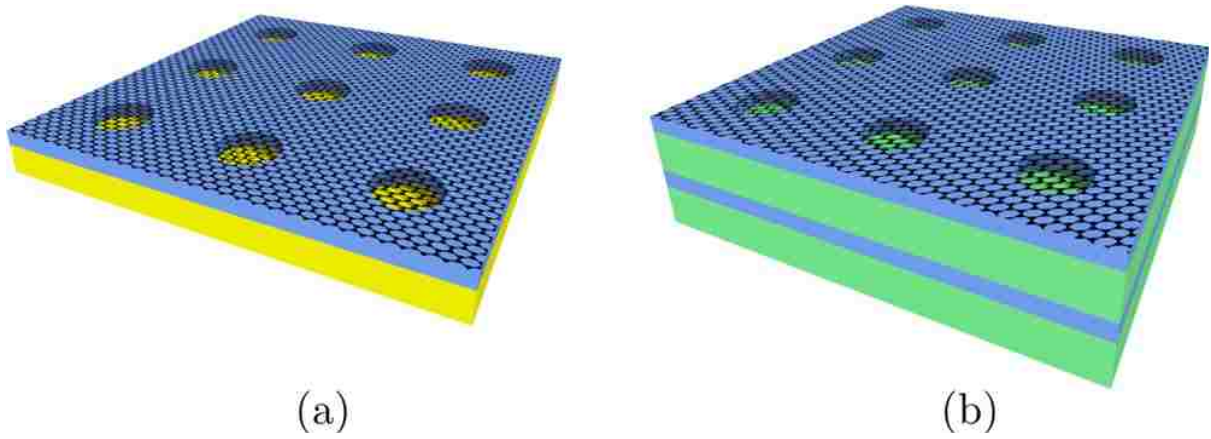In this chapter, we describe the simulation methods used for the analysis and design of the multilayer structures for the enhancement of light absorption in graphene. The transfer matrix method (TMM) is used to calculate the field distribution in the multilayer structures, and light absorption in the graphene monolayer. The layer thicknesses of the structures are optimized to maximize the absorption in the graphene monolayer using a genetic global optimization algorithm. In Section 2.2 we discuss the TMM. In Section 2.3, we discuss the genetic algorithm.

2.2 Transfer Matrix Method

Figure 2.1 is a schematic showing how the transfer matrix method is used for the analysis of the multilayer structures. Here, we assume that optical waves are propagating along the x-axis. In general, we consider structures having two multilayer stacks (M_1 and M_2 in Figure 2.1) on the left and right side of the graphene monolayer. Light is incident from air on the left side of the structure. The interface between two adjacent layers is at $x=x_i$, where the index i varies between 0 and n+m+1. For normally incident plane waves, the TM and TE modes have the same behavior. We refer thickness of ith layer as a_i.
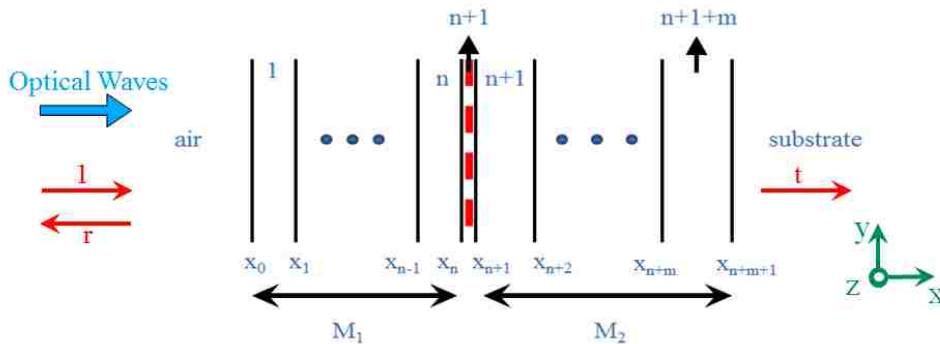

Figure 2.1 Schematic showing how the transfer matrix method is used for the analysis of the proposed structures.

For the TM polarization, the transverse components of the electric and magnetic field in each layer can be described as:

$$E_z(x,y) = (A_i e^{ik_i x} + B_i e^{-ik_i x})e^{ik_y y} \equiv E_z(x)e^{ik_y y}$$
$$H_y(x,y) = \frac{-ck_i}{Z_i \omega}(A_i e^{ik_i x} - B_i e^{-ik_i x})e^{ik_y y} \equiv H_y(x)e^{ik_y y}$$

(2-1)

Here k_y is the propagation constant in the y-direction, and is the same in all layers. In addition, k_i is the propagation constant of the waves in the x-direction in the ith layer. Z_i is equal to $\sqrt{\dfrac{\mu_0}{\varepsilon_i}}$, where $\mu_\circ$ is the free-space magnetic permeability, and ε_i is the dielectric permittivity of the material in the ith layer. Finally, A_i and B_i are the amplitudes of the forward and backward propagating waves in the ith layer, respectively. And c is speed of light in free space.

By applying the boundary conditions at the interface between air and the first layer of the structure we obtain

$$\begin{bmatrix} E_z \\ Z_0 H_y \end{bmatrix}_{X_0} = \begin{bmatrix} 1 & 1 \\ -ck_1/\omega & ck_1/\omega \end{bmatrix}\begin{bmatrix} A_1 \\ B_1 \end{bmatrix}$$

(2-2)

Similarly, by applying the boundary conditions at the second interface, we obtain

$$\begin{bmatrix} E_z \\ Z_0 H_y \end{bmatrix}_{X_1} = \begin{bmatrix} 1 & 1 \\ -ck_1/\omega & ck_1/\omega \end{bmatrix}\begin{bmatrix} e^{ik_1 X_1} & 0 \\ 0 & e^{-ik_1 X_1} \end{bmatrix}\begin{bmatrix} A_1 \\ B_1 \end{bmatrix}$$
$$= \begin{bmatrix} 1 & 1 \\ -ck_1/\omega & ck_1/\omega \end{bmatrix}\begin{bmatrix} e^{ik_1 X_1} & 0 \\ 0 & e^{-ik_1 X_1} \end{bmatrix}\begin{bmatrix} 1 & 1 \\ -ck_1/\omega & ck_1/\omega \end{bmatrix}^{-1}\begin{bmatrix} E_z \\ Z_0 H_y \end{bmatrix}_{X_0}$$
$$= \begin{bmatrix} \cos(k_1 a_1) & -i\sin(k_1 a_1) \\ -i\sin(k_1 a_1).\dfrac{ck_1}{\omega} & \cos(k_1 a_1) \end{bmatrix}\begin{bmatrix} E_z \\ Z_0 H_y \end{bmatrix}_{X_0}$$

(2-3)

Note that in Eq. (2-3), the matrix relating the transverse fields at the two interfaces of a layer is called the transfer matrix of this layer. Finally, to relate the fields in the first layer to those in the last one, we need to multiply the transfer matrices of all layers.

$$\begin{bmatrix} E_z \\ Z_0 H_y \end{bmatrix}_{X_{n+m+1}} = \begin{bmatrix} \cos(k_{n+m+1}a_{n+m+1}) & -i\sin(k_{n+m+1}a_{n+m+1}) \\ -i\sin(k_{n+m+1}a_{n+m+1}).\dfrac{ck_{n+m+1}}{\omega} & \cos(k_{n+m+1}a_{n+m+1}) \end{bmatrix} \times \dots$$
$$\begin{bmatrix} \cos(k_2 a_2) & -i\sin(k_2 a_2) \\ -i\sin(k_2 a_2).\dfrac{ck_2}{\omega} & \cos(k_2 a_2) \end{bmatrix} \begin{bmatrix} \cos(k_1 a_1) & -i\sin(k_1 a_1) \\ -i\sin(k_1 a_1).\dfrac{ck_1}{\omega} & \cos(k_1 a_1) \end{bmatrix} \begin{bmatrix} E_z \\ Z_0 H_y \end{bmatrix}_{X_0} \qquad (2\text{-}4)$$

The above equation can be rewritten as:

$$\begin{bmatrix} E_z \\ Z_0 H_y \end{bmatrix}_{X_{n+m+1}} = T \begin{bmatrix} E_z \\ Z_0 H_y \end{bmatrix}_{X_0} \qquad (2\text{-}5)$$

Considering the boundary condition for the last layer (substrate), we can derive a general formula to calculate reflection and transmission:

$$\begin{bmatrix} 1 \\ r \end{bmatrix} = \begin{bmatrix} 1 & 1 \\ -ck_1/\omega & ck_1/\omega \end{bmatrix}^{-1} T^{-1} \begin{bmatrix} 1 & 1 \\ -ck_1/\omega & ck_1/\omega \end{bmatrix} \begin{bmatrix} t \\ 0 \end{bmatrix} \qquad (2\text{-}6)$$

Since $A = 1 - |t|^2 - |r|^2$, the absorption of light in the graphene layer can be obtained, once the reflection and transmission are calculated from Eq. (2-6).

2.2.1 Condition for Perfect Absorption

Here, we consider a 1-D system consisting of a graphene monolayer sandwiched between two multilayer structures. For each of the two multilayer structures, we define a transfer matrix which relates the transverse fields at the two interfaces of the multilayer structure. We wish to derive the condition which needs to be satisfied by the transfer matrices of the two multilayer structures in order to achieve total light absorption in the graphene monolayer at a specific wavelength for normally incident light.

$$\begin{bmatrix} E_z \\ Z_0 H_y \end{bmatrix}_{X_g^l} = \begin{bmatrix} E_z \\ Z_0 H_y \end{bmatrix}_{X_n} = \begin{bmatrix} a_{11} & a_{12} \\ a_{21} & a_{22} \end{bmatrix} \begin{bmatrix} E_z \\ Z_0 H_y \end{bmatrix}_{X_0}$$
$$\begin{bmatrix} E_z \\ Z_0 H_y \end{bmatrix}_{X_g^R} = \begin{bmatrix} E_z \\ Z_0 H_y \end{bmatrix}_{X_{n+1}} = \begin{bmatrix} g_{11} & g_{12} \\ g_{21} & g_{22} \end{bmatrix} \begin{bmatrix} E_z \\ Z_0 H_y \end{bmatrix}_{X_g^l} \qquad (2\text{-}7)$$

11

$$\begin{bmatrix} E_z \\ Z_0 H_y \end{bmatrix}_{X_{n+m+1}} = \begin{bmatrix} b_{11} & b_{12} \\ b_{21} & b_{22} \end{bmatrix} \begin{bmatrix} E_z \\ Z_0 H_y \end{bmatrix}_{X_g^R}, \quad \begin{bmatrix} 1 & 1 \\ -n_s & n_s \end{bmatrix} \begin{bmatrix} T \\ 0 \end{bmatrix} = \begin{bmatrix} E_z \\ Z_0 H_y \end{bmatrix}_{X_{n+m+1}}$$

In the above equations A, G, and B are the transfer matrices of the multilayer structure on the left side of the graphene monolayer, the graphene monolayer, and the multilayer structure on the right side of the graphene monolayer, respectively. In addition, n_s is the refractive index of the substrate. Also note that in these equations x_g^l and x_g^R are equivalent to x_n and x_{n+1} in Figure 2.1.

Combining Equations (2-7), we can derive the following equation:

$$\begin{bmatrix} 1 & 1 \\ -n_s & n_s \end{bmatrix} \begin{bmatrix} T \\ 0 \end{bmatrix} = \begin{bmatrix} b_{11} & b_{12} \\ b_{21} & b_{22} \end{bmatrix} \begin{bmatrix} g_{11} & g_{12} \\ g_{21} & g_{22} \end{bmatrix} \begin{bmatrix} a_{11} & a_{12} \\ a_{21} & a_{22} \end{bmatrix} \begin{bmatrix} 1 & 1 \\ -1 & 1 \end{bmatrix} \begin{bmatrix} 1 \\ \Gamma \end{bmatrix} \qquad (2\text{-}8)$$

where Γ and T are the reflection and transmission coefficients of the multilayer structure. In order to have total absorption in the graphene monolayer, we should have: $T = \Gamma = 0$. We therefore obtain

$$\begin{bmatrix} b_{11} & b_{12} \\ b_{21} & b_{22} \end{bmatrix} \begin{bmatrix} g_{11} & g_{12} \\ g_{21} & g_{22} \end{bmatrix} \begin{bmatrix} a_{11} & a_{12} \\ a_{21} & a_{22} \end{bmatrix} \begin{bmatrix} 1 \\ -1 \end{bmatrix} = \begin{bmatrix} 0 \\ 0 \end{bmatrix} \qquad (2\text{-}9)$$

By multiplying matrices, we find:

$$\begin{aligned} a_{11}[g_{11}b_{11} + g_{21}b_{21}] + a_{21}[g_{12}b_{11} + g_{11}b_{12}] - a_{12}[g_{11}b_{11} + g_{21}b_{12}] - a_{22}[g_{12}b_{11} + g_{11}b_{12}] = 0 \\ a_{11}[g_{11}b_{21} + g_{21}b_{22}] + a_{21}[g_{12}b_{21} + g_{11}b_{22}] - a_{12}[g_{11}b_{21} + g_{21}b_{22}] - a_{22}[g_{12}b_{21} + g_{11}b_{22}] = 0 \end{aligned} \qquad (2\text{-}10)$$

Then:

$$\begin{aligned} g_{11}[a_{11}b_{11} + a_{21}b_{21} - a_{12}b_{11} - a_{22}b_{12}] + g_{12}[a_{21}b_{11} - a_{22}b_{11}] + g_{21}[a_{11}b_{12} - a_{12}b_{12}] = 0 \\ g_{11}[a_{11}b_{21} + a_{21}b_{22} - a_{12}b_{21} - a_{22}b_{22}] + g_{12}[a_{21}b_{21} - a_{22}b_{21}] + g_{21}[a_{11}b_{22} - a_{12}b_{22}] = 0 \end{aligned} \qquad (2\text{-}11)$$

And finally we obtain:

$$(a_{21} - a_{22})[g_{11}(b_{12} + b_{22}) + g_{12}(b_{11} + b_{21})] + (a_{11} - a_{12})[g_{11}(b_{11} + b_{21}) + g_{21}(b_{21} + b_{22})] = 0 \qquad (2\text{-}12)$$

2.3. Genetic Global Optimization Algorithm

The aperiodic structures described in the next chapter are designed using an optimization algorithm. Using this algorithm in combination with the transfer matrix method described in Section 2.2, we are able to optimize the layer thicknesses of the multilayer structure to maximize the absorption in the graphene monolayer at multiple prespecified wavelengths.

In this thesis, we use a genetic global optimization algorithm to get near perfect absorption for varying numbers of layers at a given wavelength, λ_0. The genetic algorithm is an iterative optimization procedure, which starts with a randomly selected population of potential solutions, and gradually evolves toward improved solutions, via the application of the genetic operators. These genetic operators are patterned after the natural selection process. In the initialization function, a population of chromosomes is created by random selection of values for the genes. The genetic algorithm then proceeds to iteratively generate a new population by the application of selection, crossover, and mutation operators [22].

More specifically, here we use the microgenetic algorithm. It has been shown that the microgenetic algorithm avoids premature convergence and shows faster convergence to the near-optimal region compared with the conventional large population genetic algorithm for multidimensional problems. The microgenetic algorithm starts with a small random population that evolves and converges after a few generations. At this point, keeping the best individual from the previously converged generation, a new random population is chosen, and the evolution process restarts. We use tournament selection as the selection scheme in the genetic algorithm. In this method, a subpopulation of individuals is randomly chosen from the population and made to compete on the basis of their fitness values. The individual in the subpopulation with the highest fitness value wins the tournament, and is thus selected. The remaining members of the entire subpopulation are then put back into the general population,

13

and the process is repeated. This selection scheme converges more rapidly and has a faster execution time compared to other competing schemes. Once a pair of individuals is selected as parents, the basic crossover operator creates two offspring by combining the chromosomes of their parents. We use uniform crossover rather than single point crossover, as it has been found that microgenetic algorithm convergence is faster with uniform crossover. An elitist strategy is also employed, wherein the best individual from one generation is passed on to the next generation [22].

CHAPTER 3
SIMULATION RESULTS

3.1. Introduction

In this chapter, interaction of light and graphene in multilayer structures will be studied. We use the Transfer Matrix Method (see chapter 2) as a tool to calculate light absorption by a graphene monolayer. In this chapter two different phenomena will be discussed. First, the possibility of multi-spectral light detection by the multilayer structures will be discussed. In addition, optimized structures to get near complete absorption will be obtained using the genetic optimization algorithm described in chapter 2. Second, we will show that the wavelength range of near total absorption can be efficiently reduced by using a design based on coupled cavities.

3.2. Multi-Spectral Light Detection

3.2.1. 1-D Periodic structure with a Single Cavity

It is shown that periodic multilayer structures can be used to achieve near total absorption in a graphene monolayer [14-21]. The proposed mechanism is very simple: we just need to place a monolayer of graphene inside an optical cavity. Periodic multilayers act as optical mirrors, and when the structure exhibits a resonance, the interaction of the graphene monolayer with the electric field is greatly enhanced. As a result, trapped optical waves inside the cavity will be absorbed by the graphene. Figure 3.1 shows the schematic of a periodic multilayer structure with a monolayer of graphene (indicated by a dashed red line) placed in the structure. As seen, the graphene layer is located between two periodic multilayer structures made of silicon (Si) and silica (SiO_2). Note that the thickness of the graphene layer is set to be 0.34 nm in all simulations [14,15] and thickness of each layer is $\lambda_0/(4n)$, where λ_0 is desired wavelength, and n is the refractive index of the material in the

layer. We use experimental data for the refractive indices of silicon and silica in all the simulations [23,24].
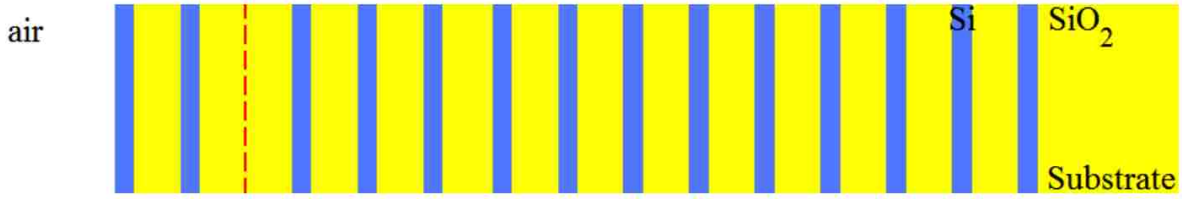

Figure 3.1 The schematic of a periodic multilayer structure with a monolayer of graphene placed inside the structure (indicated by the dashed red line). There are two pairs of Si-SiO$_2$ layers which form the left mirror and seven pairs of SiO$_2$-Si which form the right mirror. The substrate is SiO$_2$. The length of each layer is set to be $\lambda_0/(4n)$, where λ_0 is the free-space wavelength, and n is the refractive index of the material in the layer.

Figure 3.2 shows the absorption of light by the monolayer of graphene inside the periodic multilayer structure shown in Figure 3.1. It can be seen that we have only one absorption peak in the wavelength range between 1 μm and 2 μm. The length of the cavity is set to be $\lambda_o/(2n)$, where λ_0 is equal to 1.55 μm, and n is refractive index of the material in the cavity.
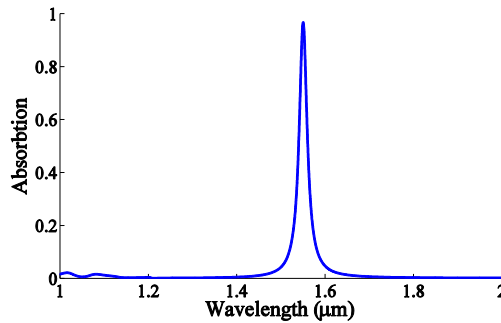

Figure 3.2. The absorption spectra of a monolayer of graphene in a periodic multilayer structure as shown in Figure 3.1.

Achieving multispectral light detection is important for many applications in photonics. In this thesis, we discuss different ways of achieving multispectral absorption of light by a monolayer of graphene. In addition, we wish to find a design approach which will enable us to achieve near total resonant light absorption in graphene at multiple wavelengths, *which can be tuned independently*.

A first approach to achieve multispectral absorption in the graphene monolayer is by increasing the thickness of the cavity sandwiched between the periodic Bragg mirrors. In fact, by increasing the thickness of the cavity, higher order resonance modes will appear in the wavelength range that we investigate. Thus, it is expected that more absorption peaks will be observed in the wavelength range of interest. For this mean, we set the thickness of the cavity equal to either 2.753 μm or 4.653 μm. Simulation results, as shown in Figure 3.3, show that we can achieve multispectral absorption peaks in the wavelength range between 1 μm and 2 μm. As seen in Figure 3.2(b), as the thickness of the cavity layer increases, the number of absorption peaks in the wavelength range of interest increases.

However, there are two facts which should be considered when using thick cavities inside the periodic structures. First, it is not possible to achieve near total light absorption for all resonances. Second, there is an important restriction for this design: we cannot independently tune the resonance wavelengths. In other words, to change the wavelength at which near total absorption is achieved, we need to change the thickness of the cavity. However, this will cause the other absorption peaks to shift to longer or shorter wavelengths because all resonances are dependent on the thickness of the cavity.
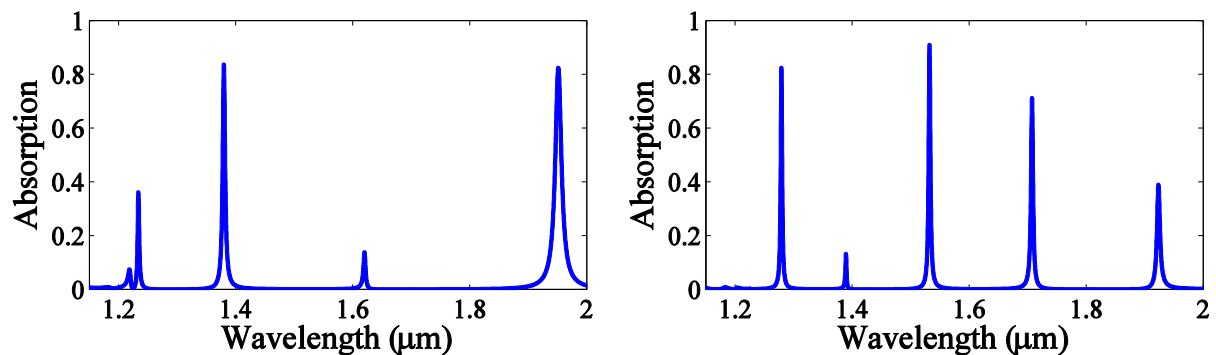

Figure 3.3. Absorption spectra of a periodic multilayer structure with one cavity (Figure 3.1) (a) The width of the cavity is (a) 2.753 μm and (b) 4.653 μm. Although this structure can support high absorption at multiple wavelengths, absorption peaks cannot be independently tuned.

3.2.2 1-D Periodic structure with two Cavities

Another design which may be helpful is using two cavities inside of a periodic structure. Locating two cavities near each other results in coupling of their resonant modes when the cavities have the same length. Here we show that a two-cavity system enables us to have near total light absorption in a graphene monolayer at two wavelengths. Using this concept, we investigate the properties of a periodic multilayer structure which includes two coupled cavities.

Figure 3.4 shows the schematic of a periodic multilayer structure which includes two cavities. We observe that the structure is similar to that of Figure 3.1, and the only difference is that one of the layers (indicated by C_2 in Figure 3.4) has a length of $\lambda_0/(2n)$. This additional defect in the periodic structure forms a second cavity. The cavities are separated by a mirror composed of periodic layers of Si and SiO_2. There should be at least one layer between these two cavities. For the structure shown in Figure 3.4 there is a mirror between the two cavities consisting of 1.5 pairs of Si-SiO_2.
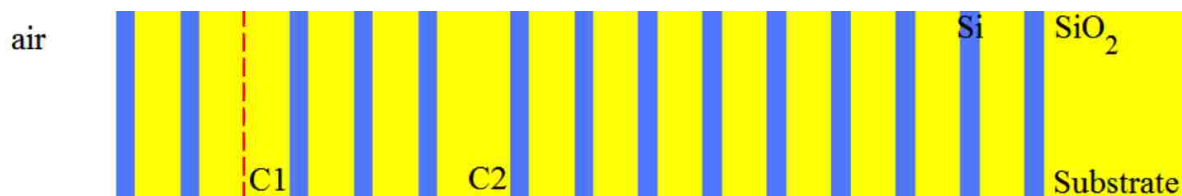

Figure 3.4 Schematic of a periodic multilayer structure which includes two cavities indicated by C_1 and C_2. The length of these cavities is $\lambda_0/(2n)$. All other parameters are as in Figure 3.1.

To show the mechanism of the two-cavity design, the spectra of a structure composed of two pairs of Si-SiO_2 as a left mirror and 6.5 pairs of Si-SiO_2 as a right mirror are shown for two cases; in the first case there is one layer of Si between two cavities (Figure 3.5(a)), and in the second case there are 7.5 pairs of Si-SiO_2 between two cavities (Figure 3.5(b)). We observe that by increasing the distance between the two cavities, the wavelengths of the absorption peaks approach 1.55 µm which is the resonance wavelength of the single cavity in

18

the absence of a second one. The reason for this behavior is that by decreasing the distance between these two cavities the coupling between them increases, and, as a result, the shift in the wavelength of the absorption peaks increases.
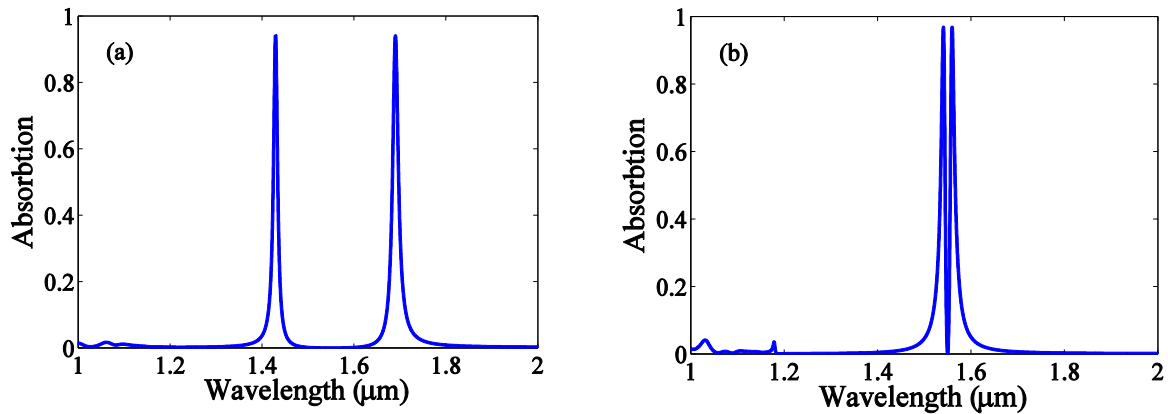

Figure 3.5. Absorption spectra of the periodic structure with two cavities of Figure 3.4. (a) There is one layer of Si between two cavities and wavelengths of the absorption peaks are at 1.43 μm and 1.69 μm. (b) There are 7.5 pairs of Si-SiO$_2$ between the two cavities and the wavelengths of the absorption peaks are at 1.54 μm and 1.56 μm.

As seen in Figure 3.5, although near total light absorption is achieved with such a structure at the two resonant wavelengths, these two wavelengths of the absorption peaks cannot be separated by more than 300 nm. Hence, a different design is required in order to achieve near total light absorption in a graphene monolayer at two wavelengths which are tunable in a broad wavelength range.
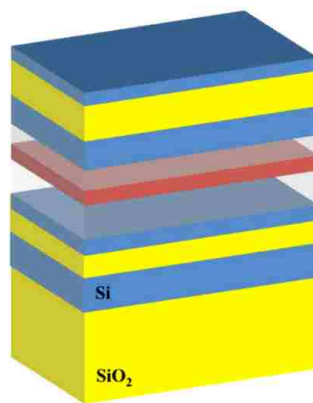
3.2.3 1-D Aperiodic structures

Schematics of the aperiodic design are shown in Figures 3.6(a) and 3.6(b). As seen, the graphene monolayer is sandwiched between two aperiodic multilayer structures composed of alternating layers of silicon and silica. The structure is deposited on a silica substrate. Here, we have designed two structures of $(HL)_n/G/(LH)_m$ or $(HL)_n/G/H(LH)_m$, where H (high refractive index), L (low refractive index), G stand for silicon, silica, and graphene, respectively; also, n and m are the numbers of the iterations. The thickness of the

graphene layer is set to be 0.34 nm as before. For simplicity we refer to the layer thicknesses

of the top and bottom structures as $\{l_1, l_2, \ldots\}_t$ and $\{l_1, l_2, \ldots\}_b$.

(a)

(b)

Figure 3.6. 1-D (a) and 3-D (b) schematics of a one-dimensional aperiodic multilayer structure. The graphene monolayer is sandwiched between two aperiodic multilayer structures composed of alternating layers of silicon and silica. The structure is deposited on a silica substrate.

As mentioned in chapter 2, the layer thicknesses are optimized using a genetic

global optimization algorithm [22] in combination with a transfer matrix method to maximize

the absorption in the graphene monolayer at multiple prespecified wavelengths. More

specifically, we maximize the fitness function $F = \sum_{i=1}^{n} A(\lambda_i)$, where $A(\lambda_i)$ is the absorption in

the graphene monolayer at normal incidence at wavelength λ_i.

We also calculated the absorption of the whole structure and found that it is

almost the same as the absorption in the graphene monolayer. This can be attributed to the

fact that the material loss of silica and silicon is negligible at the operating wavelengths

considered here. Based on this fact, it is possible to derive a condition for total light absorption in the graphene monoloayer at a specific wavelength. As described in chapter 2, we define A and B as the transfer matrices of the multilayer structures on the left and right sides of the graphene and also G as the transfer matrix of the graphene monolayer. Hence we obtain (see Sec. 2.2.1):

$$(a_{21} - a_{22})[g_{11}(b_{12} + b_{22}) + g_{12}(b_{11} + b_{21})] + (a_{11} - a_{12})[g_{11}(b_{11} + b_{21}) + g_{21}(b_{21} + b_{22})] = 0 \qquad (3\text{-}1)$$

where a_{ij}, b_{ij}, and g_{ij} are the elements of matrices A, B, and G, respectively. More details are given in Sec. 2.2.1.

3.2.3.1 Near total light absorption at two tunable wavelengths

Figures 3.7(a-d) show the absorption spectra of the $(HL)_3/G/(LH)_7$ structure. The spectra demonstrate that with such a structure it is possible to achieve near total light absorption in the graphene monolayer at two wavelengths which are tunable in a broad wavelength range. It turns out that, when the structure is optimized at two wavelengths λ_1 and λ_2, it can achieve near total resonant light absorption in the graphene monolayer at these wavelengths. We observe that these two resonances can be simultaneously tuned in a broad wavelength range extending from ~1200 nm to ~1900 nm (Figures 3.7 (a-d)).

In Figures 3.8(a) and 3.8(b) we show the profile of the electric field amplitude, normalized with respect to the field amplitude of the incident plane wave, for the genetic algorithm-optimized system described in Figures 3.7(b). The structure is excited by a normally incident plane wave at either $\lambda_1=1.2$ μm or $\lambda_2=1.9$ μm. We observe a large resonant enhancement of the electric field at the graphene monolayer, which leads to near total light absorption in graphene on resonance (Figures 3.7(b)). While the field patterns of the two resonant modes are very different, they lead to approximately the same field enhancement at the graphene monolayer.
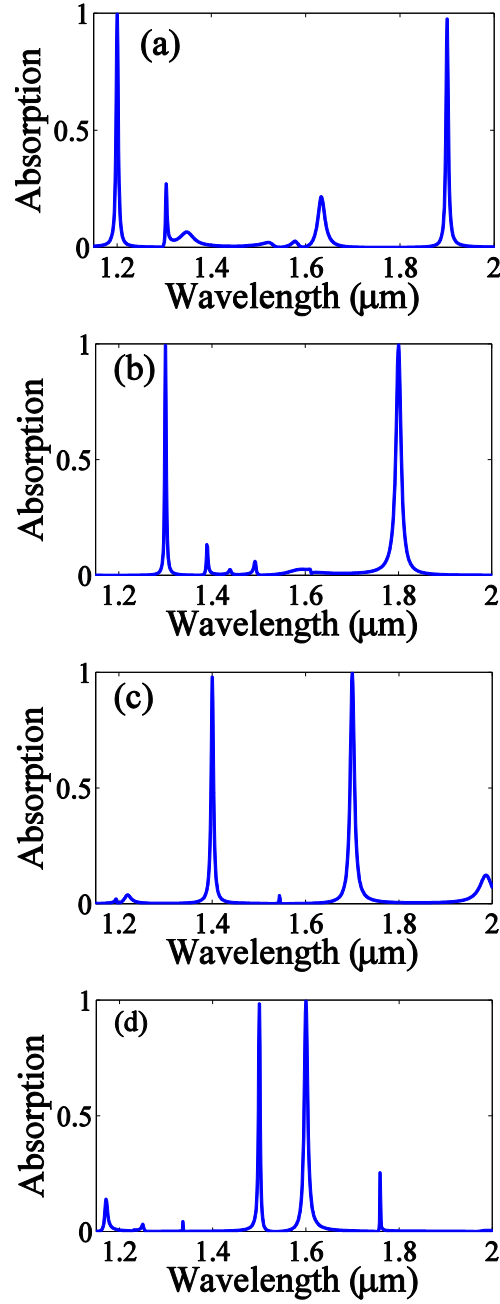
Figure 3.7. Absorption in the graphene monolayer of optimized structures as a function of wavelength at normal incidence for the $(HL)_3/G/(LH)_7$ structure: (a) $\lambda_1=1.2$ µm and $\lambda_2=1.9$ µm. The layer thicknesses are $\{218.2, 341.3, 380.1, 279.6, 432.7, 201.4\}_t$ and $\{177.4, 253.5, 315.1, 195.3, 974.4, 110.5, 257.6, 419.1, 257.2, 417.4, 257.9, 419.1, 257.2, 598.2\}_b$. (b) $\lambda_1=1.3$ µm and $\lambda_2=1.8$ µm. The layer thicknesses are $\{188.2, 201.1, 192.2, 153.3, 262.3, 187.7\}_t$ and $\{277.1, 153.7, 255.5, 295.8, 474.1, 130.1, 157.1, 512.9, 237.2, 391.1, 212.1, 432.6, 217.1, 528.2\}_b$. (c) $\lambda_1=1.4$ µm and $\lambda_2=1.7$ µm. The layer thicknesses are $\{118.2, 61.4, 180.8, 219.9, 368.9, 131.3\}_t$ and $\{117.4, 353.5, 215.2, 295.5, 573.1, 120.1, 212.4, 312.6, 274.3, 423.8, 212.2, 509.2, 303.2, 603.1\}_b$. (d) $\lambda_1=1.5$ µm and $\lambda_2=1.6$ µm. The layer thicknesses are $\{143.2, 192.4, 50.5, 343.1, 156.4, 186.6\}$ and $\{318.7, 320.3, 276.1, 449.3, 724.2, 545.1, 283.5, 324.7, 255.3, 117.4, 253.6, 110.8, 257.8, 600\}$.
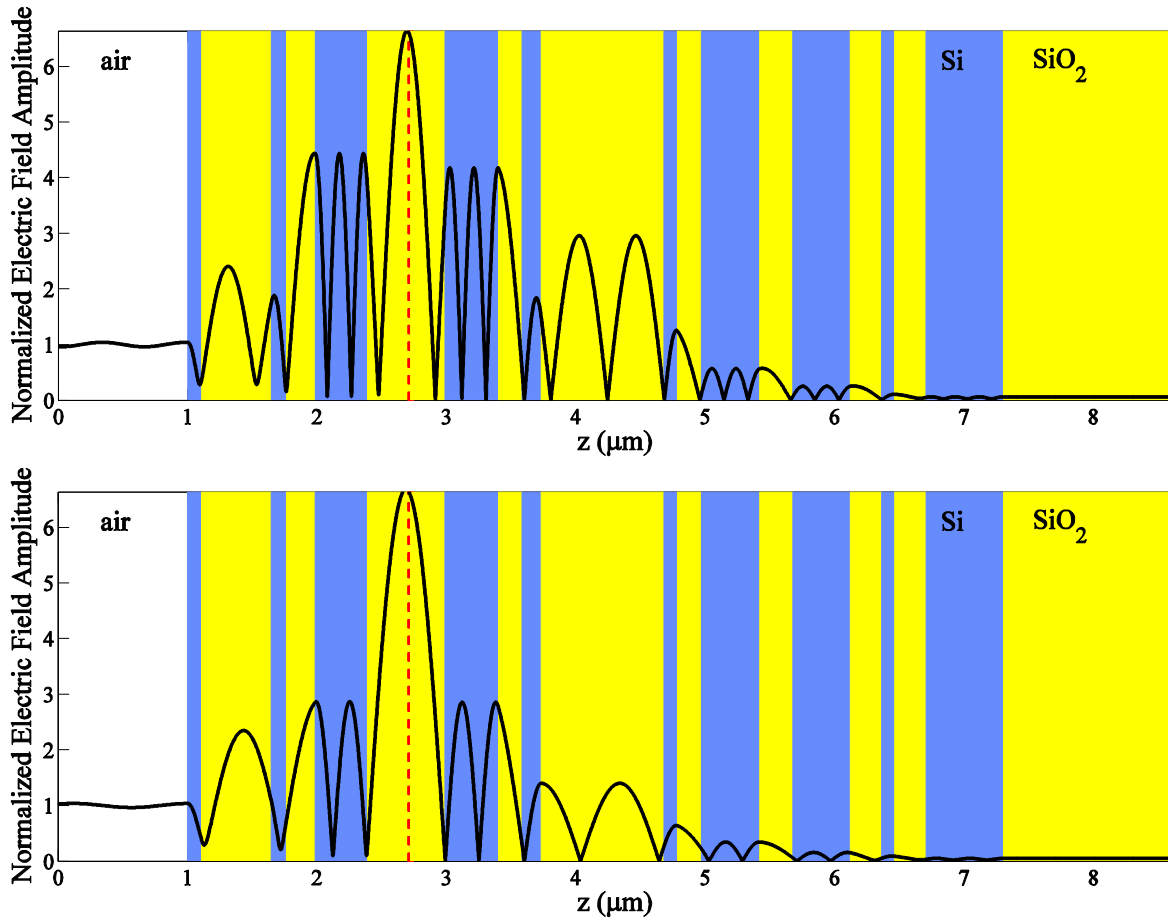*Note*: the layer thicknesses are in units of nanometers.

22

Figure 3.8 Profile of the electric field amplitude, normalized with respect to the field amplitude of the normally incident plane wave for the $(HL)_3/G/(LH)_7$ structure described in Figure 3.7(b). The red dashed line indicates the position of the graphene monolayer. The resonant wavelengths of absorption are (a) $\lambda_1=1.3$ μm. (b) $\lambda_2=1.8$ μm.

3.2.3.2. Near total light absorption at three tunable wavelengths

To shed light on the high tunability properties of aperiodic designs, we investigate the structures optimized at three wavelengths λ_1, λ_2, and λ_3. As seen in Figures 3.9(a-d) more than ~90% of the incident light is resonantly absorbed in the graphene monolayer at these wavelengths. As in the previous case, the three resonances can be simultaneously tuned in a broad wavelength range extending from ~1200 nm to ~1900 nm (Figures 3.9 (c), 3.9 (d)). It should be noted that in this case the central wavelength is fixed at 1550 nm, and the other two wavelengths of the absorption peaks are varied. Such absorption tunability in a broad

wavelength range cannot be achieved by previously proposed structures, such as those reported in References 15 and 16.

In Figures 3.10(a) and 3.10(b) we show the profile of the electric field amplitude, normalized with respect to the field amplitude of the incident plane wave, for the genetic algorithm optimized system described in Figure 3.9(a). The structure is excited by a normally incident plane wave at λ_1=1.2 μm, λ_2=1.55 μm, and λ_3=1.9 μm. We observe a large resonant enhancement of the electric field at the graphene monolayer, which leads to near total light absorption in graphene on resonance (Figure 3.9(a)).
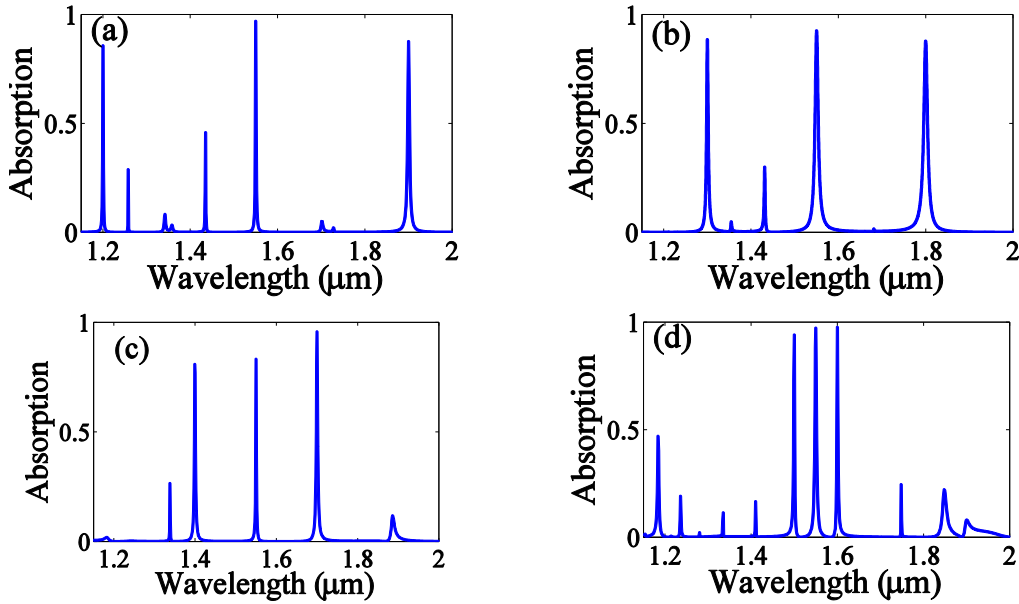

Figure 3.9. Absorption in the graphene monolayer of optimized structures as a function of wavelength at normal incidence for (a) (HL)$_3$/G/ (LH)$_7$: $\lambda_{1,3} = \lambda_2 \pm 350$ nm, $\lambda_2 = 1550$ nm. The layer thicknesses are: {101.8, 257.1, 737.3, 479.2, 472.7, 285.1}$_t$ and {493.3, 528.8, 144.9, 899.4, 355.5, 344.3, 464.1, 427.5, 116.9, 282.9, 931.4, 231.2, 101.8, 220.4, 600}$_b$. (b) (HL)$_3$/G/(LH)$_6$: $\lambda_{1,3} = \lambda_2 \pm 250$ nm, $\lambda_2 = 1550$ nm. The layer thicknesses are: {108.2, 254.9, 106.1, 518, 427.5, 276.5}$_t$ and { 258.6, 136.3, 99.6, 437.5, 184.1, 977.6, 326.1, 119, 222.5, 103.9, 246.3, 600}$_b$. (c) (HL)$_3$/G/H(LH)$_6$: $\lambda_{1,3} = \lambda_2 \pm 150$ nm, $\lambda_2 = 1550$ nm. The layer thicknesses are: {321.8, 270, 315.3, 237.6, 410.2, 339}$_t$ and { 206.5, 300.2, 462, 284.7, 564.1, 228.8, 121.2, 252.7, 114.7, 261.4, 112.5, 263.5, 600}$_b$. (d) (HL)$_3$/G/(LH)$_7$: $\lambda_{1,3} = \lambda_2 \pm 50$ nm, $\lambda_2 = 1550$ nm. The layer thicknesses are: {388.6, 564.7, 168.6, 185.9, 86.6, 295.9}$_t$ and {824.9, 306.7, 177.3, 880.8, 947.8, 1000, 515.9, 550.4, 254.9, 323.9, 254.9, 116.9, 254.9, 600}$_b$. Note: the layer thicknesses are in units of nanometers.
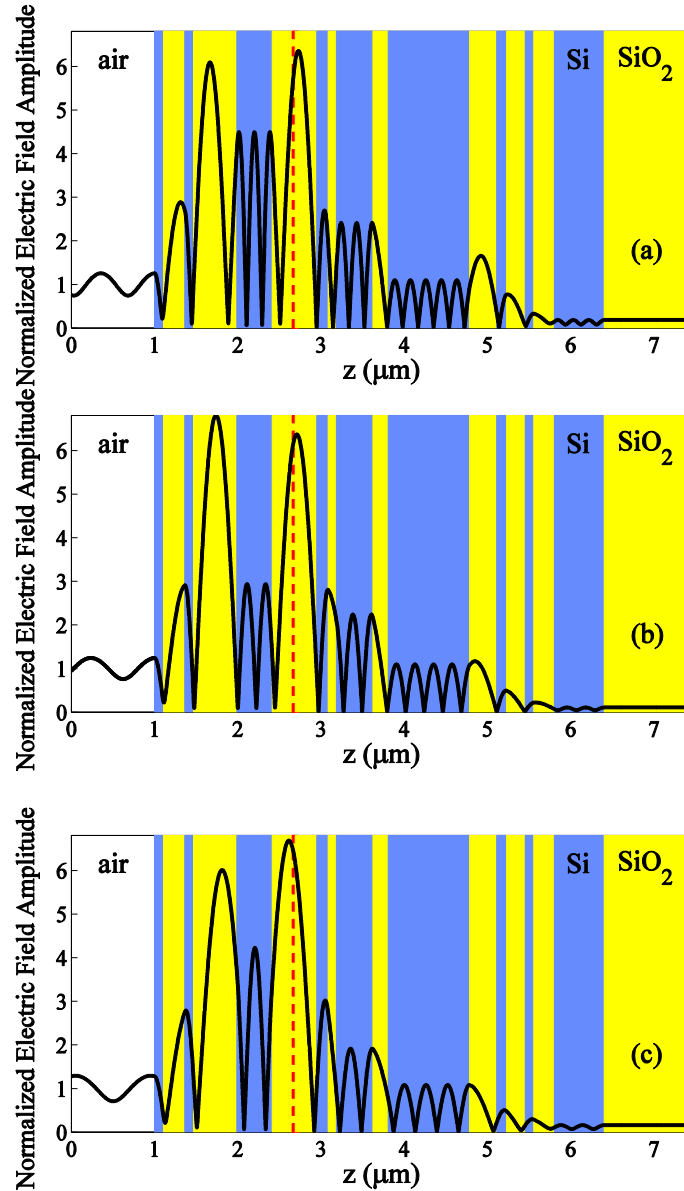
Figure 3.10. Profile of the electric field amplitude, normalized with respect to the field amplitude of the normally incident plane wave for the structure described in Figure 3.9(b). The red dashed line indicates the position of the graphene monolayer. The resonant wavelengths of absorption are (a) λ_1=1.3 μm. (b) λ_2=1.55 μm (c) λ_2=1.8 μm.

We also show that the aperiodic design can be applied to obtain similar behavior in other wavelength ranges. To show this, we designed structures exhibiting near total light absorption in a graphene monolayer at two tunable wavelengths in the wavelength range 0.75 μm-0.95 μm. The simulation results are shown in Figures 3.11(a-b). We used the same materials for the layers as in Ref. 15. Here, the bottom mirror includes 25 periods of

alternating layers of AlAs and $Al_{0.10}Ga_{0.90}As$ as in Ref. 15. Moreover, we used 13 and 10 layers with aperiodic thicknesses on the left and right side of the graphene, respectively. As shown in Figures 3.11(a-b) we can effectively control the wavelengths of the absorption peaks.
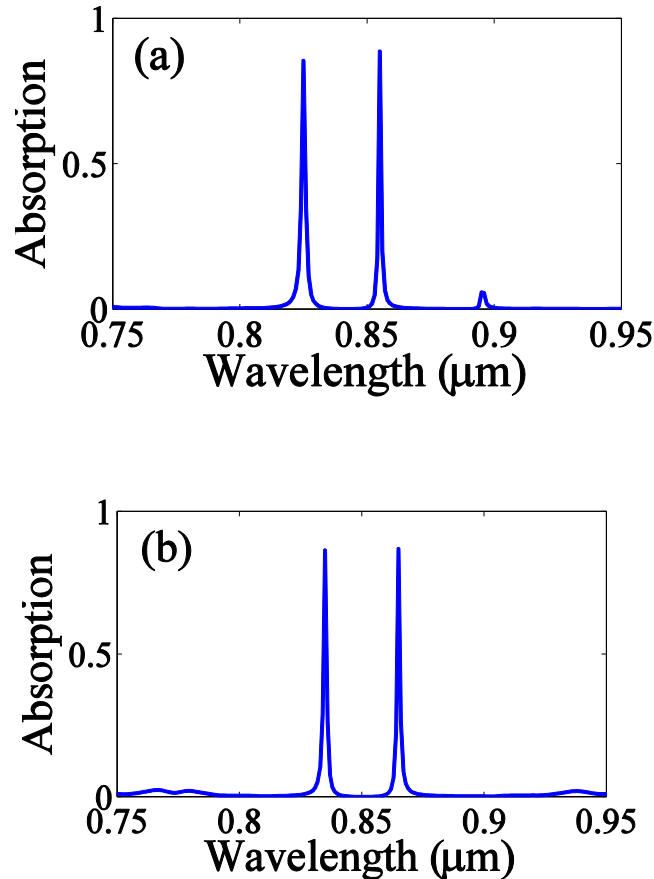

Figure 3.11. Absorption in the graphene monolayer of optimized structures as a function of wavelength at normal incidence for (a) λ_1=0.825 μm and λ_2=0.855 μm. The layer thicknesses are: {125.2, 438.4, 343.4, 124.3, 127.2, 132.1, 125.2, 138.2, 114.5, 141.9, 360.1, 429.5, 310.2, 176.1}$_t$ and {90.1, 130.1, 85.1, 156.6, 131.1, 359.1, 79.2, 316, 242.7, 424.7, 453.2, 122.8}$_b$. (b) λ_1=0.835 μm and λ_2=0.865 μm. The layer thicknesses are: {115.3, 328.1, 143.5, 104.3, 231.5, 119.2, 142.7, 186.6, 112.5, 153.2, 321.9, 392.1, 210.9, 116.2}$_t$ and {125, 152.7, 105.3, 86.7, 129.3, 309.9, 69.4, 316, 218.9, 482.2, 383, 111.5, }$_b$. Note that these layers are deposited on the 25 periods of layers of AlAs (with thickness of 61 nm) and $Al_{0.10}Ga_{0.90}As$ (with thickness of 70 nm). Note: the layer thicknesses are in units of nanometers.

Another point to mention is that during the fabrication process the thicknesses of the layers may not be the same as those used in the simulations. As a result, there might be a shift in the wavelengths of the absorption peaks. However, we found that this shift can be

compensated by changing the angle of the incident wave. Tunability of multilayered structures based on the angle of the incident waves is discussed in Refs. 20-24.

3.2.3.3. Effect of incident angle on absorption peaks

In the previous sections we showed that aperiodic multilayer structure designs enable us to achieve near total absorption in a graphene monolayer at multiple wavelengths which are tunable in a broad wavelength range. In all these simulations it was assumed that we have normally incident light. As a result, in all cases the absorption is the same for both transverse magnetic (TM) and transverse electric (TE) modes. Here, we will investigate the properties of aperiodic multilayer structures when the optical waves illuminate the structures at different angles ranging from 0 to 90 degrees.

The layer thicknesses are the same as those of the structures described in Sections 3.2.3.1 and 3.2.3.2. Figures 3.12 and 3.13 show the absorption spectra as a function of the angle of incidence for the aperiodic multilayer structures designed to exhibit near total light absorption at normal incidence in a graphene monolayer at two or three tunable wavelengths.

As seen in Figure 3.12, in all cases the absorption is almost constant for angles of incidence less than five degrees. When the angle of incidence increases, the absorption decreases. This is due to the fact that the wavelengths of the absorption peaks shift. We also observe that in general the absorption for the TE mode is larger than the absorption for the TM mode for angles larger than 65 degrees. Especially for an operating wavelength of 1.9 μm (Figure 3.12(b)) we observe high absorption for the TE mode in a broad angular range. Another phenomenon which is seen in Figure 3.12 is the existence of additional absorption resonances for both TE and TM modes in the angular range of 40 to 50 degrees.

We also did similar calculations for the aperiodic multilayer structures which exhibit near total light absorption in the graphene monolayer at three wavelengths shown in

Figure 3.13. As in the previous case, we observe that in many cases for angles larger than 65 degrees the absorption in the graphene monolayer is high in a broad angular range for the TE mode. In contrast, the TM mode exhibits additional narrow absorption peaks. For example, as seen in Figure 3.13(b), the TM mode has a sharp absorption peak around 75 degrees, while the TE mode exhibits high absorption in a much broader wavelength range. For angles between 40 and 50 degrees we observe that both modes have high and narrow absorption peaks.
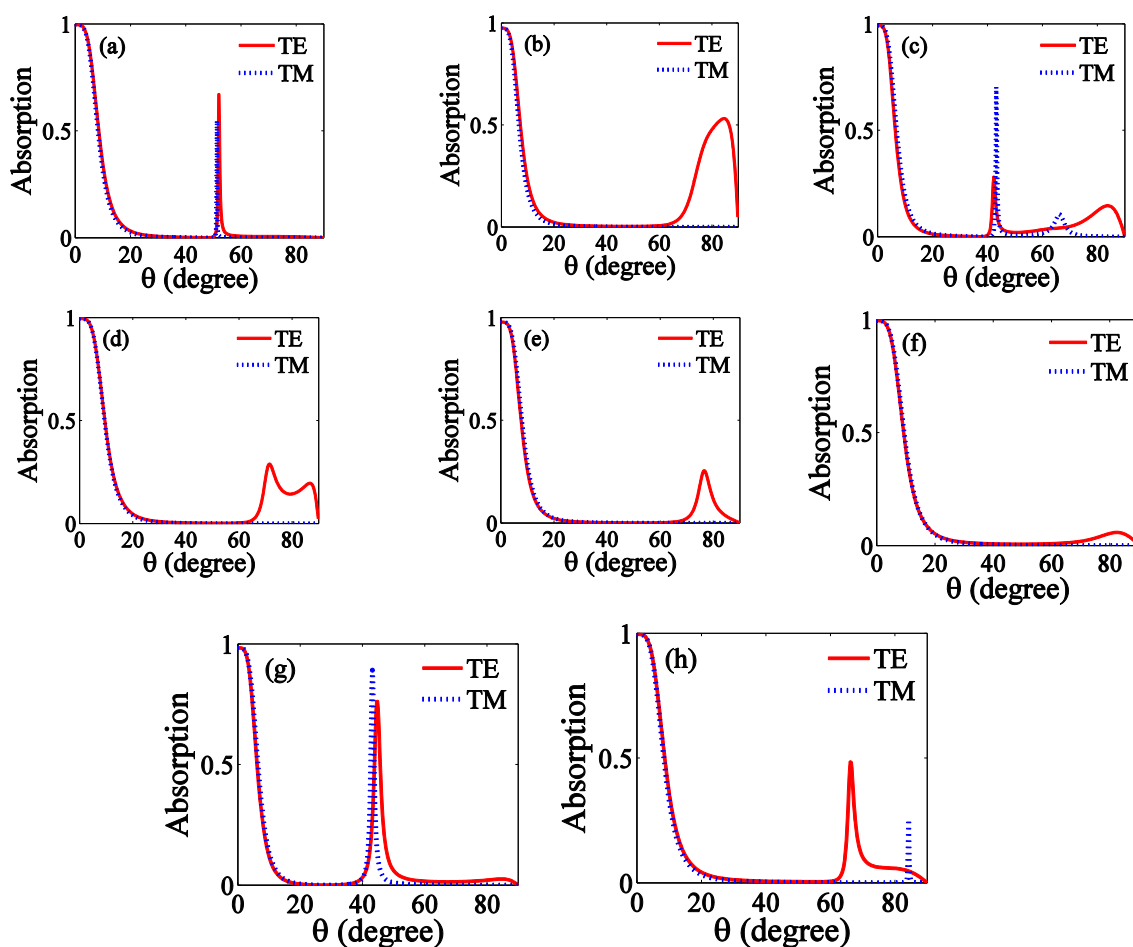

Figure 3.12. Absorption of aperiodic multilayer structures as a function of the angle of incident light at the following wavelengths: (a) λ = 1.2 μm, (b) λ = 1.9 μm, (c) λ = 1.3 μm, (d) λ = 1.8 μm, (e) λ = 1.4 μm, (f) λ = 1.7 μm, (g) λ = 1.5 μm, (h) λ = 1.6 μm. These results corrrespond to the aperiodic multilayer structures designed to exhibit near total light absorption at normal incidence in a graphene monolayer at two tunable wavelengths (see Figure 3.7).
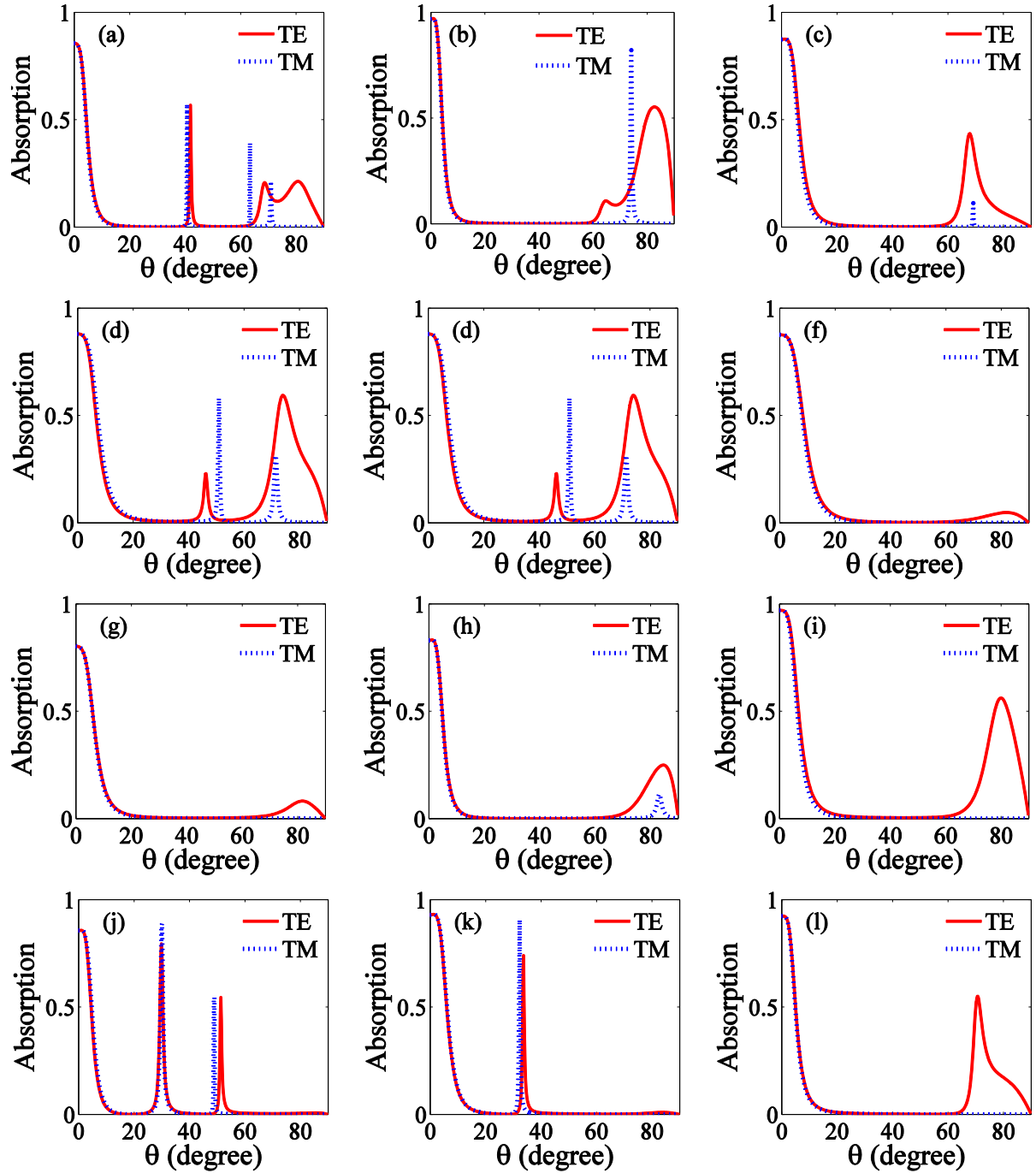
Figure 3.13. Absorption of aperiodic multilayer structures as a function of the angle of incident light at the following wavelengths: (a) λ = 1.2 μm, (b) λ = 1.55 μm, (c) λ = 1.9 μm, (d) λ = 1.3 μm, (e) λ = 1.55 μm, (f) λ = 1.8 μm, (g) λ = 1.4 μm, (h) λ = 1.55 μm, (i) λ = 1.7 μm, (j) λ = 1.5 μm, (k) λ = 1.55 μm, (l) λ = 1.6 μm. These results corrrespond to the aperiodic multilayer structures designed to exhibit near total light absorption at normal incidence in a graphene monolayer at three tunable wavelengths (see Figure 3.9).

3.3. Near total light absorption in an ultra narrow wavelength range

One of the reasons that graphene has attracted a lot of attention as an optical material is its potential applications in nonlinear optics [18,20]. As reported in Refs. 17 and 19, the large third-order nonlinearity of graphene when combined with large field enhancement in a graphene layer could lead to controllable, saturable absorption at the pump frequency. For these types of applications, it is important to achieve high absorption in the graphene monolayer in a narrow wavelength range. It is therefore of interest to investigate whether multilayer structures such as those described in the previous sections could lead to near total light absorption in a graphene monolayer in an ultra narrow wavelength range.

To the best of our knowledge, so far, no method has been proposed to enable the design of a multilayer structure with a monolayer of graphene which exhibits near total absorption in an ultra narrow wavelength range. In this thesis, a method is proposed to greatly decrease the bandwidth of the absorption resonance in a graphene monolayer embedded in a multilayer structure.

In pervious works [14-21], the graphene monolayer was located inside or next to a cavity (defect) in which the electric field is greatly enhanced. Since graphene is a lossy material, the interaction of light and graphene in the cavity considerably affects the quality factor of the resonator and decreases it. The concept that we use here is to introduce a second resonator which is weakly coupled to the resonator containing the graphene monolayer. If for the mode that leads to high absorption in graphene, the peak of the field enhancement is in this second resonator, then the width of the absorption resonance could become ultra narrow.

Figure 3.14 shows the schematic of our design. As seen, we have created two cavities inside of a periodic multilayer structure. The graphene monolayer is embedded in the first cavity. Also, there are two pairs of Si-SiO$_2$ layers on the left of the structure, 2.5 pairs of Si-

SiO$_2$ layers between the two cavities, and 8.5 pairs of Si-SiO$_2$ layers between the second
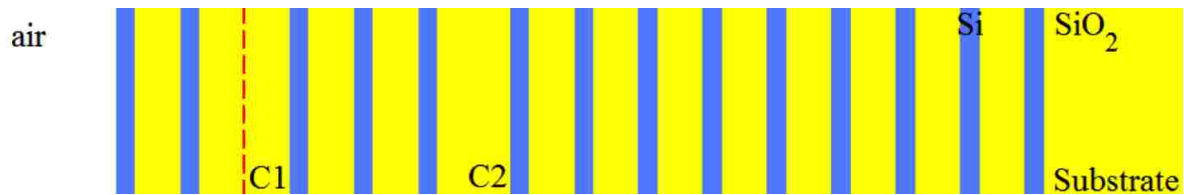
cavity and the substrate.

Figure 3.14. Schematic of a periodic multilayer structure which includes two cavities. A monolayer of graphene has been located in the first cavity. There are two pairs of Si-SiO$_2$ layers on the left of the structure, 2.5 pairs of Si-SiO$_2$ layers between the two cavities, and 8.5 pairs of Si-SiO$_2$ layers between the second cavity and the substrate. The length of the first and second cavity is $\lambda_o/2n$ and $\lambda_o/2.5n$, respectively.

Figure 3.15 shows the absorption spectra in the graphene monolayer inside the

designed structure. As seen, there are two absorption peaks at 1.55 μm and 1.75 μm. It is

obvious that the absorption peak at 1.55 μm is narrower than the absorption peak at 1.75 μm;

the quality factor Q of the first absorption resonance is ~2822, while the quality factor of the

second one is only ~70.1. Thus, in the proposed structure the spectral width of one of the

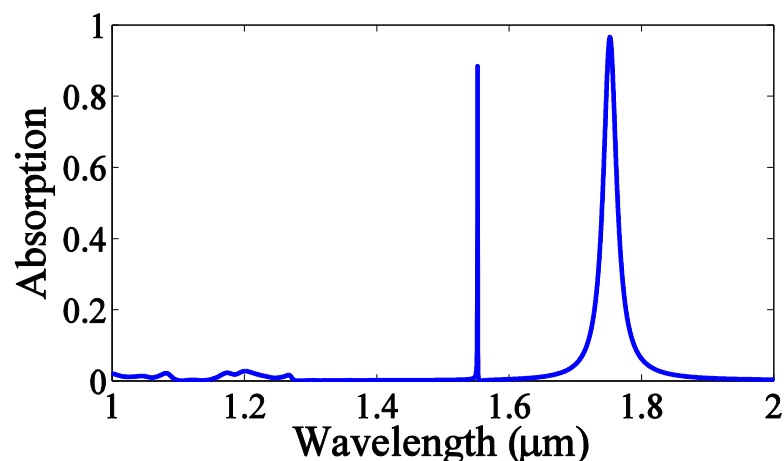resonances is about 40 times narrower than the width of the second resonance.

Figure 3.15. Absorption spectra of a monolayer of graphene in a periodic multilayer structure with two cavities as in Figure 3.14. All parameters are as in Figure 3.14.

For better understanding of this behavior the electric fields profiles corresponding to

these two absorption peaks have been plotted in Figure 3.16. As shown in Figure 3.16(a),

which is related to the narrower absorption peak at 1.55 μm, the electric field peak is in the second cavity and the field intensity in the cavity containing the graphene monolayer is significantly lower. On the other hand, for the 1.75 μm peak (Figure 3.16(b)), the electric fields are concentrated in the first cavity where the graphene monolayer is located.
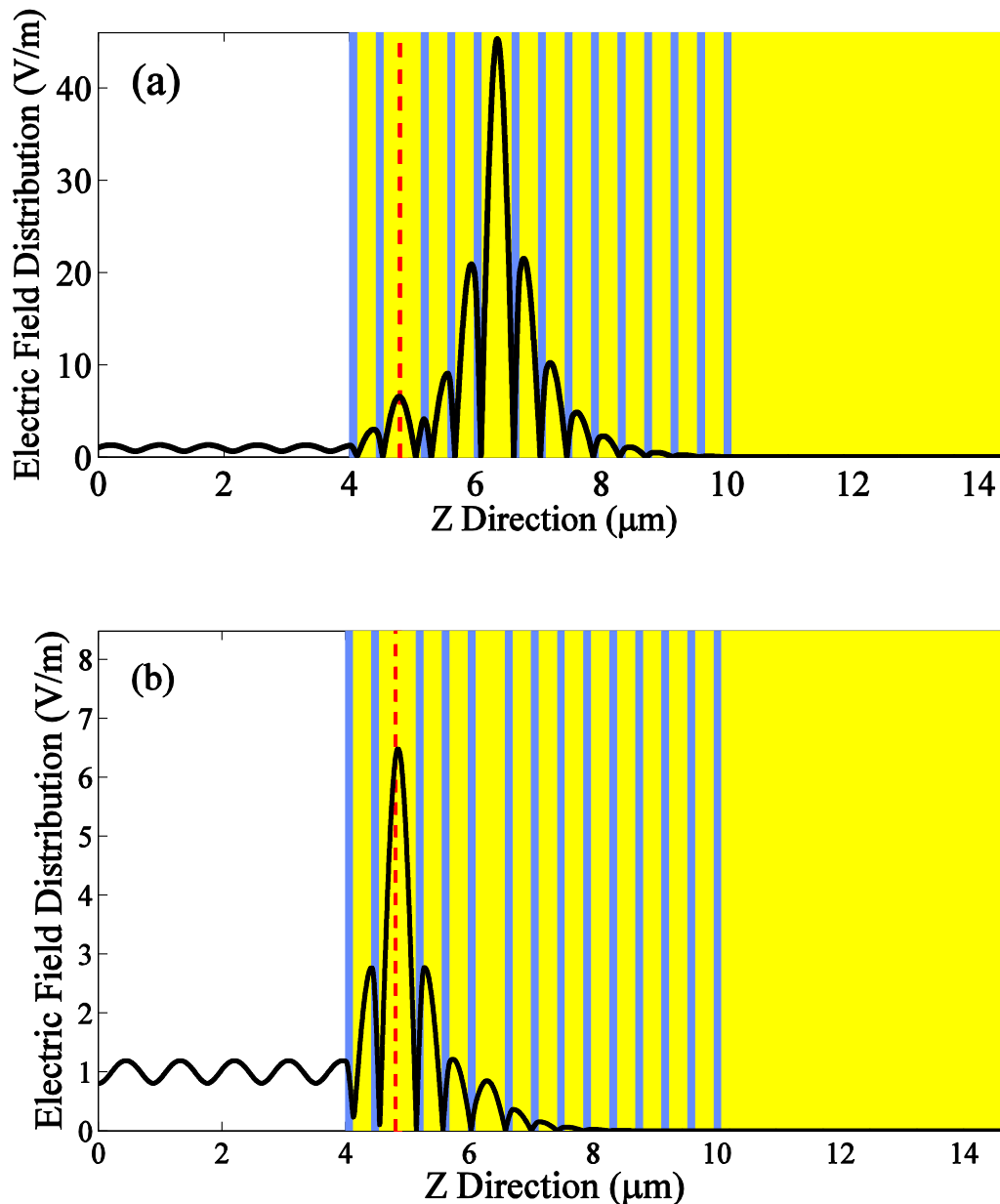

Figure 3.16. Profile of the electric field amplitude, normalized with respect to the field amplitude of the normally incident plane wave for the structure described in Figure 3.15(b). The red dashed line indicates the position of the graphene monolayer. The resonant wavelengths of absorption are (a) λ_1=1.55 μm. (b) λ_2=1.75 μm.

CHAPTER 4
CONCLUSIONS & FUTURE WORK

In this thesis, aperiodic multilayer structures were introduced as an efficient design to get highly controllable near total absorption of light by a monolayer of graphene at multiple tunable wavelengths. We showed that tunable double and triple absorption peaks can be obtained in a wide wavelength range extending from 1200 nm to 1900 nm for a structure using layers of silicon and silica. This feature is useful for multispectral light detection. Using different materials, it is also possible to design such structures at different wavelength ranges. Also, a new design was proposed to achieve narrow peaks in graphene absorption spectra, which could be important for nonlinear optics applications of graphene. The Transfer Matrix Method coupled to a genetic global optimization algorithm was used for the analysis of the optical structures and to find the structure parameters for near perfect absorption.

One of the potential future research directions is to consider cylindrical multilayer structures. In such structures one could use graphene as the top layer, which is suitable for fabrication processes. It is expected that by using such a design it will be possible to obtain optical resonance modes with fields concentrated below the graphene layer. It would also be interesting to investigate 1-D optical logic gates using two cavity defects in multilayer structures.

From the computational point of view, more efficient methods can be used to optimize multilayer structures. Using hybrid optimization algorithms, which combine global and local optimization methods, could significantly accelerate the design process.

REFERRNCES

[1] C. Binns, "Introduction to Nanoscience and Nanotechnology," (John Wiley, 2010).

[2] J. H. Warner, F. Schaffel, and M. Rummeli "Graphene: Fundamentals and emergent applications," (Elsevier 2013).

[3] Z. Liu and X. Zhou, "Graphene: Energy Storage and Conversion Applications," (CRC Press, 2015).

[4] S. Rumyantsev, G. Liu, M. S. Shur, R. A. Potyrailo, and A. A. Balandin, "Selective Gas Sensing with a Single Pristine Graphene Transistor," ACS Nano **12**, 2294–2298 (2012).

[5] B. Zhan, C. Li, J. Yang, G. Jenkins, W. Huang, and X. Dong, "Graphene Field-Effect Transistor and Its Application for Electronic Sensing," Small **10**, 4042–4065 (2014).

[6] A. Pospischil, M. Humer, M. M. Furchi, D. Bachmann, R. Guider, T. Fromherz, and T. Mueller, "CMOS-compatible graphene photodetector covering all optical communication bands," Nature Photonics **7**, 892-896 (2013).

[7] Q. Bao and K. P. Loh, "Graphene photonics, plasmonics, and broadband optoelectronic devices," ACS Nano **6**, 3677−3694 (2012).

[8] W. D. Tan, C. Y. Su, R. J. Knize, G. Q. Xie, L. J. Li, and D. Y. Tang "Mode locking of ceramic Nd:yttrium aluminum garnet with graphene as a saturable absorber," Appl. Phys. Lett. **96**, 031106 (2010).

[9] T. Mueller, F. Xia, and P. Avouris, "Graphene photodetectors for high-speed optical communications," Nat. Photonics **4**, 297-301 (2010).

[10] M. Liu, X. Yin, E. Ulin-Avila, B. Geng, and T. Zentgraf, "Plasmon resonance enhanced multicolour photodetection by graphene," Nat. Commun. **2**, 579−585 (2011).

[11] L. Ju, F. Wang, and X. Zhang "A graphene-based broadband optical modulator," Nature **474**, 64-67 (2011).

[12] Z. Sun, T. Hasan, F. Torrisi, D. Popa, G. Privitera, F. Wang, F. Bonaccorso, D. M. Basko, and A. C. Ferrari "Graphene mode-locked ultrafast laser," ACS Nano **4**, 803-810 (2010).

[13] T. J. Echtermeyer, L. Britnell, P. K. Jasnos, A. Lombardo, R. V. Gorbachev, A. N. Grigorenko, A. K. Geim, A. C. Ferrari, and K. S. Novoselov "Strong plasmonic enhancement of photovoltage in graphene," Nat. Commun. **2**, 1-5 (2011).

[14] M. Furchi, A. Urich, A. Pospischil, G. Lilley, K. Unterrainer, H. Detz, P. Klang, A. M. Andrews, W. Schrenk, G. Strasser, and T. Mueller "Microcavity-Integrated Graphene Photodetector," Nano Lett. **12**, 2773-2777 (2012).

[15] J. R. Piper and S. Fan "Total Absorption in a Graphene Monolayer in the Optical Regime by Critical Coupling with a Photonic Crystal Guided Resonance," ACS Photonics **1**, 347-353 (2014).

[16] M. A. Vincenti, D. de Ceglia, M. Grande, A. D'Orazio, and M. Scalora "Third-harmonic generation in one-dimensional photonic crystal with graphene-based defect," Phys. Rev. B. **89**, 165139 (2014).

[17] R. Miloua, Z. Kebbab, F. Chiker, M. Khadraoui, K. Sahraoui, A. Bouzidi, M. Medles, C. Mathieu, and N. Benramdane "Peak, multi-peak and broadband absorption in graphene-based one-dimensional photonic crystal," Optics Commun. **330**, 135-139 (2014).

[18] M. A. Vincenti, D. de Ceglia, M. Grande, A. D'Orazio, and M. Scalora "Nonlinear control of absorption in one-dimensional photonic crystal with graphene-based defect," Opt. Lett. **38**, 3550-3553 (2013)**.**

[19] B. Vasić and R. Gajić "Tunable Fabry–Perot resonators with embedded graphene from terahertz to near-infrared frequencies," Opt. Lett. **39**, 6253-6256 (2014).

[20] J.-T. Liu, N.-H. Liu, J. Li, X. J. Li, and J.-H. Huang "Enhanced absorption of graphene with one-dimensional photonic crystal," App. Phys. Lett. **101**, 052104 (2012).

[21] M. Grande, M. A. Vincenti, T. Stomeo, D. de Ceglia, V. Petruzzelli, M. De Vittorio, M. Scalora, and A. D'Orazio "Absorption and losses in one dimensional photonic crystal based absorbers incorporating graphene," IEEE Photonics. **99**, 1-6 (2014).

[22] C. H. Granier, F. O. Afzal, C. Min, J. P. Dowling, and G. Veronis, "Optimized aperiodic highly directional narrowband infrared emitters," J. Opt. Soc. Am. B **31**, 1316-1321 (2014).

[23] M. Bruna and S. Borini, "Optical constants of graphene layers in the visible range," Appl. Phys. Lett. **94**, 031901 (2009).

[24] D. R. Lide, CRC Handbook of Chemistry and Physics, 88th ed. (CRC Press, 2007).

VITA

Iman Zand is a native of Tehran (Iran), and received his bachelor's degree at K. N. Toosi University in December 2011. He went on to become a graduate student at Louisiana State University in the Division of Electrical and Computer Engineering. He anticipates to receive his master's degree in December 2015.